The effective spin concept to analyze coherent charge transport in mesoscopic systems

J. Wan, W. Liu, and M. Cahay
Department of Electrical and Computer Engineering, University of Cincinnati, Cincinnati, Ohio 45221

V. Gasparian
Department of Physics, California State University, Bakersfield, California 93311

S. Bandyopadhyay
Department of Electrical and Computer Engineering, Virginia Commonwealth University, Richmond, Virginia 23284

(Received 19 September 2009; accepted 14 September 2010)

The concept of effective spin is introduced to underpin the fundamental isomorphism between two apparently disparate fields of physics—phase coherent charge transport in mesoscopic systems and qubit operations in a spin-based quantum logic gate. Together with the Bloch sphere concept, this isomorphism allows transport problems to be formulated in a language more familiar to workers in spintronics and quantum computing. We exemplify the application of the effective spin concept by formulating several charge transport problems in terms of specific unitary operations (rotations) of a spinor on the Bloch sphere. © *2011 American Association of Physics Teachers.*
[DOI: 10.1119/1.3531938]

I. INTRODUCTION

Two major areas of research that have evolved somewhat independently over the past three decades are phase coherent charge transport in mesoscopic structures (ultrasmall structures smaller than the inelastic mean free path of an electron)[1–4] and quantum computing based on coherent rotations of an electron spin.[5–15] These two areas are seemingly disparate because one deals with the charge degree of freedom of an electron and the other with the spin degree of freedom, but there are some similarities which suggest that there may be a fundamental connection between them. For example, phase coherence of the electron's wave function is needed in both applications. For charge transport the orbital part of the electron's wave function needs to retain phase coherence, and for spin-based quantum computing the spin part of the wave function needs to remain phase coherent. Because of these similarities, a unified description should exist that applies to both fields.

Some recent efforts have been made to stress the analogies between coherent charge transport and coherent spin operations,[16,17] but that description is couched in a language that is too sophisticated to teach at the undergraduate level in most physics or engineering curricula. In this article we have steered clear of sophisticated jargon and difficult concepts and instead used materials from undergraduate level physics to explain the effective spin concept, which is the theoretical tool that connects charge transport and spin qubit operation. Hopefully, this article will inspire inquisitive students to delve further into the fields of coherent charge transport and spin qubit operations.

We first show how the wave function of an electron incident on a mesoscopic structure can be written as a 2×1 component spinor instead of the usual scalar and how the wave function of the transmitted electron can also be written as a 2×1 component spinor. Next we show that the 2×2 scattering matrix that relates the transmitted wave function spinor to the incident wave function spinor can be interpreted as the unitary matrix describing the coherent rotation of a spin whose initial state corresponds to the incident wave and whose final state corresponds to the transmitted wave. Passage of the electron through the mesoscopic structure can therefore be viewed as coherent spin rotation. This viewpoint allows us to unify the fields of coherent charge transport and spin-based operations.

Ionicioiu[16] formulated a similar approach to describe the phenomenon of entanglement (a concept much discussed in the context of spin-based quantum computing) between propagating modes in a mesoscopic structure. This entanglement has been observed by Neder *et al.*[17]

The outline of this paper is as follows. In Sec. II we introduce the effective spin concept to describe coherent transport due to a single channel in mesoscopic systems in which an arbitrary tunneling problem is characterized by the electron transmission and reflection amplitude as a function of the incident energy. In Sec. III we describe the quantum computing analog to the tunneling problem and introduce the very important concept of the Bloch sphere. Section IV contains several numerical examples to illustrate this analogy by revisiting single channel charge tunneling through a single delta scatterer, a resonant tunneling structure, a periodic array of delta scatterers, and one-dimensional (1D) arrays of randomly distributed elastic scatterers using the language of quantum computing.

II. THE EFFECTIVE SPIN CONCEPT

In tunneling problems the mesoscopic structure through which an electron tunnels is characterized by an arbitrary potential barrier. The transmission and reflection amplitudes are usually calculated by the scattering matrix approach.[18,19] The scattering matrix relates the incoming (a^+,b^-) to outgoing (b^+,a^-) wave amplitudes on both sides of a scattering region (mesoscopic structure), as shown in Fig. 1, such that

$$|\psi(\mathrm{OUT})\rangle=\begin{bmatrix}b^+\\a^-\end{bmatrix}=S\begin{bmatrix}a^+\\b^-\end{bmatrix}=\begin{bmatrix}t & r'\\ r & t'\end{bmatrix}\begin{bmatrix}a^+\\b^-\end{bmatrix}=S|\psi(\mathrm{IN})\rangle, \tag{1}$$

where S is the scattering matrix.

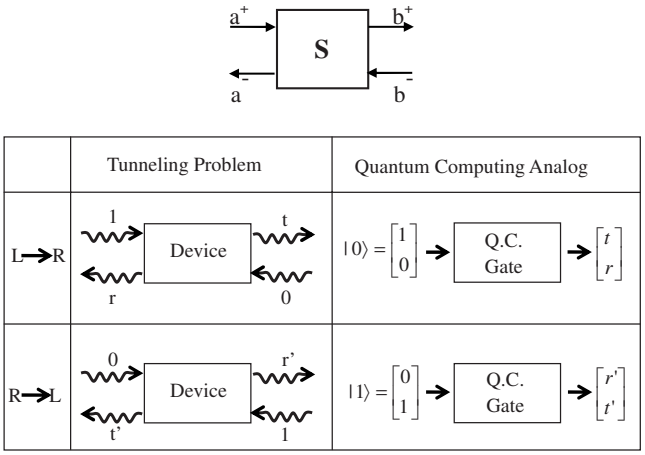

Fig. 1. The tunneling problem and its quantum computing gate equivalent. The scattering matrix associated with a device relates the incoming (a^+, b^-) to the outgoing (a^-, b^+) wave amplitudes. It can be interpreted as the matrix representing the rotation of a qubit from the initial state $|\psi(\mathrm{IN})\rangle$ to the final state $|\psi(\mathrm{OUT})\rangle$.

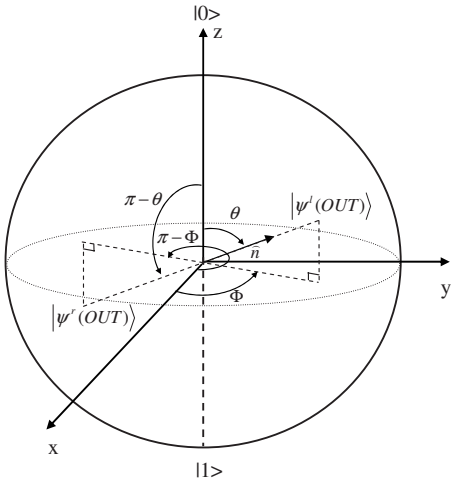

Fig. 2. Bloch sphere representation of the effective spin (qubit) $|\psi(\mathrm{OUT})\rangle$. The radius of the sphere is equal to 1. $|\psi(\mathrm{OUT})\rangle$ ($|\psi'(\mathrm{OUT})\rangle$) is the spinor given in Eq. (3) [Eq. (5)] when the electron is incident from the left (right) contact.

For single-mode transport, assuming an electron incident from the left,

$$|\psi(\mathrm{IN})\rangle = \begin{bmatrix} 1 \\ 0 \end{bmatrix} \tag{2}$$

and

$$|\psi(\mathrm{OUT})\rangle = \begin{bmatrix} t \\ r \end{bmatrix}, \tag{3}$$

whereas for an electron incident from the right, we have

$$|\psi'(\mathrm{IN})\rangle = \begin{bmatrix} 0 \\ 1 \end{bmatrix} \tag{4}$$

and

$$|\psi'(\mathrm{OUT})\rangle = \begin{bmatrix} r' \\ t' \end{bmatrix}. \tag{5}$$

The tunneling problem is completely characterized by the amplitudes (t, r) or (r', t') depending on the direction of incidence of the incoming electron.

Without loss of generality, we can always think of the two-component column vector $|\psi(\mathrm{OUT})\rangle$ as a spinor because it is normalized for coherent transport. The normalization follows from the unitarity of the scattering matrix, that is, $S^\dagger S = I$ († represents the Hermitian conjugate). Furthermore, the spinor $|\psi(\mathrm{OUT})\rangle$ can be thought of as the output of a one-qubit quantum gate whose input is the spinor $|\psi(\mathrm{IN})\rangle = (1,0)^\dagger$ or $(0,1)^\dagger$ depending on the direction of propagation of the incident electron. The 2×2 unitary matrix linking the spinors $|\psi(\mathrm{IN})\rangle$ and $|\psi(\mathrm{OUT})\rangle$ can therefore be viewed as the matrix characterizing the rotation of a qubit whose initial state was $|\psi(\mathrm{IN})\rangle$ and whose final state is $|\psi(\mathrm{OUT})\rangle$. This matrix is also the scattering matrix describing the tunneling problem. Herein lies the analogy between a quantum logic operation on a spin qubit and coherent charge transport in a mesoscopic structure.

III. QUANTUM COMPUTING ANALOG

Consider the tunneling problem of an electron incident from the left on an arbitrary one-dimensional conduction band energy profile $E_c(x)$. We refer to the (2×1) column vector $|\psi(\mathrm{OUT})\rangle$ in Eq. (3) as the *effective spin* whose components characterize completely the scattering amplitudes of the tunneling electron. For an arbitrary potential energy profile $E_c(x)$, the amplitude $|\psi(\mathrm{OUT})\rangle$ can be found by successively cascading scattering matrices associated with subsections within each of which $E_c(x)$ is approximated by constant values $E_{c1}, E_{c2}, E_{c3}, \ldots, E_{cn}$.[18,19] The evolution of the pure state $|\psi(\mathrm{OUT})\rangle$ after crossing a number of subsections can be represented using the Bloch sphere concept in which the spinor is parametrized as[7,20]

$$|\psi(\mathrm{OUT})\rangle = e^{i\gamma}\left[\cos\frac{\theta}{2}|0\rangle + \sin\frac{\theta}{2}e^{i\varphi}|1\rangle\right], \tag{6}$$

where γ is an arbitrary phase factor and the angles (φ, θ) are the azimuthal and polar angles, as shown in Fig. 2.

In Eq. (6), $|0\rangle$ and $|1\rangle$ are the (2×1) column vectors $(1,0)^\dagger$ and $(0,1)^\dagger$, respectively, associated with the north and south poles of the Bloch sphere. They are mutually orthogonal, that is, their inner product $\langle 0|1\rangle = 0$.[7]

To complete the effective spin picture, we consider the 2×2 matrix,[21]

$$\rho = |\psi(\mathrm{OUT})\rangle\langle\psi(\mathrm{OUT})| = \begin{pmatrix} t \\ r \end{pmatrix}(t^* r^*) = \begin{pmatrix} |t|^2 & tr^* \\ rt^* & |r|^2 \end{pmatrix}. \tag{7}$$

Using this density matrix and the Pauli spin matrices $(\sigma_x, \sigma_y, \sigma_z)$, the effective spin components associated with the spinor $|\psi(\mathrm{OUT})\rangle$ are given by

$$\langle S_x\rangle = \frac{\hbar}{2}\mathrm{Tr}(\rho\sigma_x) = \frac{\hbar}{2}(tr^* + rt^*) = \hbar\ \mathrm{Re}(rt^*) = \hbar\ \mathrm{Re}(r^* t), \tag{8}$$

$$\langle S_y\rangle = \frac{\hbar}{2}\mathrm{Tr}(\rho\sigma_y) = \frac{\hbar}{2}i(tr^* - rt^*) = \hbar\ \mathrm{Im}(rt^*) = -\hbar\ \mathrm{Im}(r^*t), \tag{9}$$

and

$$\langle S_z\rangle = \frac{\hbar}{2}\mathrm{Tr}(\rho\sigma_z) = \frac{\hbar}{2}(|t|^2 - |r|^2) = \frac{\hbar}{2}(1-2|r|^2) = \frac{\hbar}{2}(2|t|^2 - 1). \tag{10}$$

For an electron incident from the right, $|\psi'(\mathrm{IN})\rangle = |1\rangle$, and the density matrix $\rho'(=|\psi'(\mathrm{OUT})\rangle\langle\psi'(\mathrm{OUT})|)$ is such that $\rho' = 1-\rho$, where ρ is given by Eq. (7) and the components $\langle S_x\rangle$, $\langle S_y\rangle$, and $\langle S_z\rangle$ are the negative of the values in Eqs. (8)–(10). Therefore, the two spinors corresponding to $|\psi'(\mathrm{OUT})\rangle$ and $|\psi'(\mathrm{OUT})\rangle$ are mirror images of each other, corresponding to a reflection through the origin of the Bloch sphere. As a result, $|\psi'(\mathrm{OUT})\rangle$ and $|\psi'(\mathrm{OUT})\rangle$ are orthogonal, which they must be because the scattering matrix is unitary.

The unitarity of the scattering matrix also leads to

$$\langle S_x\rangle^2 + \langle S_y\rangle^2 = \hbar^2|t|^2(1-|t|^2) \tag{11}$$

and

$$\langle S_x\rangle^2 + \langle S_y\rangle^2 + \langle S_z\rangle^2 = \hbar^2/4. \tag{12}$$

Equation (11) shows that the projection of the spinor in the equatorial plane of the Bloch sphere reaches a maximum when $|t| = |r| = 1/\sqrt{2}$. Actually, $\langle S_x\rangle^2 + \langle S_y\rangle^2$ is proportional to $|t|^2(1-|t|^2)$, that is, the low frequency shot noise power for the tunneling electron.[22] Because $\langle S_x\rangle$, $\langle S_y\rangle$, and $\langle S_z\rangle$ are proportional to the components of the spinor $|\psi(\mathrm{OUT})\rangle$ on the Bloch sphere, Eq. (12) states that the spinor stays on the Bloch sphere during the cascading of the scattering matrices. The latter are unitary for the case of coherent transport. The angles $(\gamma, \theta, \varphi)$ appearing in the generic expression of the spinor (or qubit) in Eq. (6) can be expressed in terms of the phases and magnitudes of the reflection and transmission coefficients,

$$|\psi'(\mathrm{OUT})\rangle = \begin{bmatrix} t \\ r \end{bmatrix} = \begin{bmatrix} |t|e^{i\phi_T} \\ |r|e^{i\phi_R} \end{bmatrix} = e^{i\phi_T}\begin{bmatrix} |t| \\ |r|e^{i(\phi_R - \phi_T)} \end{bmatrix}, \tag{13}$$

where ϕ_R and ϕ_T are the phases of the reflection and transmission amplitudes, respectively. We obtain $\gamma = \phi_T$ and $\varphi = \phi_R - \phi_T$. Furthermore,

$$|t| = \cos\frac{\theta}{2}, \tag{14}$$

$$|r| = \sin\frac{\theta}{2} = \sqrt{1-|t|^2}, \tag{15}$$

and therefore

$$\frac{\theta}{2} = \tan^{-1}\left(\frac{|r|}{|t|}\right). \tag{16}$$

Equations (8)–(10) are therefore equivalent to

$$\langle S_x\rangle = \frac{\hbar}{2}\sin\theta\cos\varphi, \tag{17}$$

$$\langle S_y\rangle = \frac{\hbar}{2}\sin\theta\sin\varphi, \tag{18}$$

and

$$\langle S_z\rangle = \frac{\hbar}{2}\cos\theta. \tag{19}$$

Equations (8) and (9) show that the averages $\langle S_x\rangle$ and $\langle S_y\rangle$ contain more information than the sample conductance alone. The latter depends only on the magnitude of the transmission $|t|$ or reflection $|r|$ in the Landauer picture,[23] whereas $\langle S_x\rangle$ and $\langle S_y\rangle$ depend on the phase relation between t and r as well. The phase relation is a strong function of the energy of the incident electron. At nonzero temperature, there will be a thermal spread in the energy of the incident electron which will lead to a decrease with temperature of the average spin components $\langle S_x\rangle$ and $\langle S_y\rangle$, that is, the off-diagonal components of the density matrix ρ. Note that although $\langle S_x\rangle$ and $\langle S_y\rangle$ depend on the off-diagonal components of the density matrix and are very energy sensitive, $\langle S_z\rangle$ depends only on the diagonal components of the density matrix and is much less energy sensitive.

The 2×2 unitary matrix or quantum computing gate U_{QG}, which relates $|\psi(\mathrm{OUT})\rangle$ and $|\psi(\mathrm{IN})\rangle$ on the Bloch sphere, has the general form,[7]

$$U_{\mathrm{QG}}(\alpha,\beta,\eta,\zeta) = e^{i\alpha}R_z(\beta)R_y(\eta)R_z(\zeta), \tag{20}$$

where $(\alpha,\beta,\eta,\zeta)$ are real numbers and the R_y and R_z are the 2×2 matrices associated with rotations of the spinor on the Bloch sphere about the $\hat{y}$ and $\hat{z}$ axes, respectively. If we use the fact that $R_y(\eta) = e^{-i\eta\sigma_y/2}$ and $R_z(\zeta) = e^{-i\zeta\sigma_z/2}$,[7] we obtain

$$U_{\mathrm{QG}}(\alpha,\beta,\eta,\zeta) = \begin{bmatrix} e^{i(\alpha-\beta/2-\zeta/2)}\cos\frac{\eta}{2} & -e^{i(\alpha-\beta/2+\zeta/2)}\sin\frac{\eta}{2} \\ e^{i(\alpha+\beta/2-\zeta/2)}\sin\frac{\eta}{2} & e^{i(\alpha+\beta/2+\zeta/2)}\cos\frac{\eta}{2} \end{bmatrix}. \tag{21}$$

For $|\psi'(\mathrm{IN})\rangle = |0\rangle$ we have

$$|\psi'(\mathrm{OUT})\rangle = U_{\mathrm{QG}}(\alpha,\beta,\eta,\zeta)|0\rangle = \begin{bmatrix} e^{i(\alpha-\beta/2-\zeta/2)}\cos\frac{\eta}{2} \\ e^{i(\alpha+\beta/2-\zeta/2)}\sin\frac{\eta}{2} \end{bmatrix}, \tag{22}$$

which is the special case of a spinor on the Bloch sphere in Eq. (6), corresponding to

$$\alpha = \gamma = \phi_T, \tag{23a}$$

$$\eta = \theta = 2\tan^{-1}\left[\frac{|r|}{|t|}\right], \tag{23b}$$

$$\beta = -\zeta = \varphi = \phi_R - \phi_T. \tag{23c}$$

Hence, from a quantum computing perspective, the analytical expression for U_{QG} is identical to the scattering matrix used to described the tunneling problem and is given by

$$U_{\mathrm{QG}}(\phi_T,\theta,|t|)=e^{i\phi_T}R_z(\phi_R-\phi_T)R_y \times\left(2\tan^{-1}\left[\frac{|r|}{|t|}\right]\right)R_z(\phi_T-\phi_R). \tag{24}$$

Equation (24) helps visualizing coherent charge transport (or tunneling) through specific mesoscopic devices as a successive set of rotations of the effective spin on the Bloch sphere.

IV. EXAMPLES

A. Scattering across a single delta scatterer

We first determine the quantum computing gate analog of a simple delta scatterer of strength $V_I\delta(x)$ for which the reflection and transmission amplitudes are easily shown to be

$$t'=t=\frac{ik}{ik-k_0}=\frac{i\tilde{k}}{i\tilde{k}-1} \tag{25}$$

and

$$r'=r=\frac{k_0}{ik-k_0}=\frac{1}{i\tilde{k}-1}, \tag{26}$$

with $\tilde{k}=k/k_0$, $k_0=m^*V_I/\hbar^2$, and $k=\sqrt{2m^*E/\hbar^2}$; E is the kinetic energy of the electron and m^* is its effective mass.

The magnitude and phase of t and r are therefore

$$|t|=\frac{\tilde{k}}{\sqrt{\tilde{k}^2+1}},\quad \phi_T=-\tan^{-1}\left(\frac{1}{\tilde{k}}\right) \tag{27}$$

and

$$|r|=\frac{1}{\sqrt{\tilde{k}^2+1}},\quad \phi_R=\tan^{-1}(\tilde{k})-\pi. \tag{28}$$

The spinor $|\psi'(\mathrm{OUT})\rangle$ for this problem is given by Eq. (6), where

$$\varphi=\phi_R-\phi_T=-\frac{\pi}{2} \tag{29}$$

and

$$\theta=2\tan^{-1}(1/\tilde{k}). \tag{30}$$

The equivalent quantum computing gate is characterized by the unitary matrix U_{QG} given by

$$U_{\mathrm{QG}}=e^{i\varphi_T}R_z\left(\frac{-\pi}{2}\right)R_y(\theta)R_z\left(\frac{\pi}{2}\right)=e^{i\varphi_T}R_x(-\theta), \tag{31}$$

where R_x is the matrix for spinor rotation about the x axis.[7] For low incident energy, $\theta=\pi$ and θ monotonically go to 0 as the energy of the incident electron increases. According to Eqs. (17)–(19) the spinor $|\psi'(\mathrm{OUT})\rangle$ sweeps out only a very limited portion of the Bloch sphere, that is, the semicircle in the y-z plane, going from the south to north poles clockwise as the energy of the incident electron increases. The spin components of $|\psi'(\mathrm{OUT})\rangle$ along the x, y, and z axes are given by

$$\langle S_x\rangle=0, \tag{32}$$

$$\langle S_y\rangle=-\frac{\hbar}{2}\left(\frac{2\tilde{k}}{\tilde{k}^2+1}\right), \tag{33}$$

and

$$\langle S_z\rangle=\frac{\hbar}{2}\left(\frac{\tilde{k}^2-1}{\tilde{k}^2+1}\right). \tag{34}$$

For instance, when $\tilde{k}=1$, $|\psi'(\mathrm{OUT})\rangle$ is in the equatorial plane of the Bloch sphere along the y axis. In this case $\theta=\pi/2$, and the matrix U_{QG} is given by

$$U_{\mathrm{QG}}=e^{-i(\pi/4)}R_z\left(-\frac{\pi}{2}\right)R_y\left(\frac{\pi}{2}\right)R_z\left(\frac{\pi}{2}\right) =e^{-i\pi/4}S\left(-\frac{\pi}{2}\right)\sigma_x\mathcal{H}S\left(\frac{\pi}{2}\right), \tag{35}$$

where

$$S(\delta)=\begin{bmatrix}1 & 0\\ 0 & e^{i\delta}\end{bmatrix} \tag{36}$$

and

$$\mathcal{H}=\frac{1}{\sqrt{2}}\begin{bmatrix}1 & 1\\ 1 & -1\end{bmatrix} \tag{37}$$

are, respectively, the general phase shift and the Hadamard matrix, which are extensively used in the theory of quantum computing.[7]

B. Scattering through a delta scatterer in a region of length a

Next, we consider the scattering problem across a region of length a containing a delta function scatterer at location x_0. The corresponding scattering matrix can be derived. The location of the spinor $|\psi'(\mathrm{OUT})\rangle$ on the Bloch sphere is described by the azimuthal angle θ given in Eq. (30) and the polar angle

$$\varphi=-\frac{\pi}{2}-k(a-2x_0). \tag{38}$$

The average values of the effective spin components are given by

$$\langle S_x\rangle=\frac{\hbar}{2}\left(\frac{2\tilde{k}}{\tilde{k}^2+1}\right)\sin k(2x_0-a), \tag{39a}$$

$$\langle S_y\rangle=-\frac{\hbar}{2}\left(\frac{2\tilde{k}}{\tilde{k}^2+1}\right)\cos k(2x_0-a), \tag{39b}$$

$$\langle S_z\rangle=\frac{\hbar}{2}\left(\frac{\tilde{k}^2-1}{\tilde{k}^2+1}\right). \tag{39c}$$

In this case $\langle S_x\rangle$ is nonzero unless $x_0=a/2$, that is, unless the potential energy profile in the device is spatially symmetric. For a fixed value of the incident wave vector, the spinor $|\psi'(\mathrm{OUT})\rangle$ moves on a circle parallel to the (x,y) plane. If a is selected such that $ka=\pi$, φ increases linearly from $-3\pi/2$ to $\pi/2$ as x_0 varies from 0 to a; that is, the Bloch vector

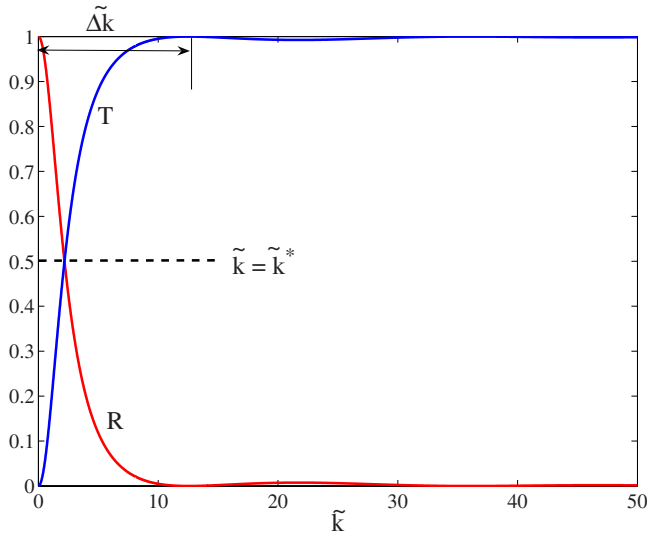

Fig. 3. Transmission ($T=|t|^2$) and reflection ($R=|t|^2$) coefficients for an electron incident on a resonant tunneling structure as a function of the reduced wave vector $\tilde{k}=k/k_0$, where $k=\sqrt{2m^*E/\hbar^2}$, E is the kinetic energy of the incident electron in the contact, and $k_0=m^*V_I/\hbar^2$, V_I is the strength of the delta scatterer. The two delta function scatterers are separated by 50 Å and have a strength $V_I=0.3$ eV Å. $\Delta\tilde{k}$ is the minimum wave vector (in reduced units) needed to realize a spin flip from the south to north poles on the Bloch sphere.

associated with the spinor sweeps the entire plane defined by the component $\langle S_z\rangle$. According to Eqs. (39a) and (39b), if $ka=\pi$, the average values of $\langle S_x\rangle$ and $\langle S_y\rangle$ are equal to zero when we average over the impurity location x_0. This is a requirement in the theory of localization in 1D arrays of scatterers, as will be discussed later.

The quantum computing gate U_{QG} analog of this tunneling problem is given by

$$U_{\mathrm{QG}} = e^{i\phi_T}R_z\left(-\frac{\pi}{2}+k(2x_0-a)\right)R_y(\theta)R_z \times\left(k(a-2x_0)+\frac{\pi}{2}\right). \tag{40}$$

Because θ is still given by Eq. (30), a spin flip from the south to the north pole is possible only if we increase the energy of the incident electron to infinity. The energy cost for the spin flip is drastically reduced if we have two or more delta scatterers, as we will discuss next.

C. Scattering across a resonant tunneling structure

We consider the scattering problem across a resonant tunneling structure consisting of two delta function scatterers of equal strength V_I separated by a distance a. In our numerical calculations we use $V_I=0.3$ eV Å and $a=50$ Å. Figure 3 is a plot of the transmission coefficient T as a function of the reduced wave vector $\tilde{k}$. The first two resonances (at which $T=1$) occur at $\tilde{k}\approx 12.5$ and 36. The corresponding variation of the phase angles (φ,θ) for the spinor $|\psi(\mathrm{OUT})\rangle$ is displayed in Fig. 4. The angle θ reaches its minimum value of zero at the resonances when there is a sudden jump in φ. When viewed as a quantum computing gate, a resonant tunneling device is more efficient when operated over the range

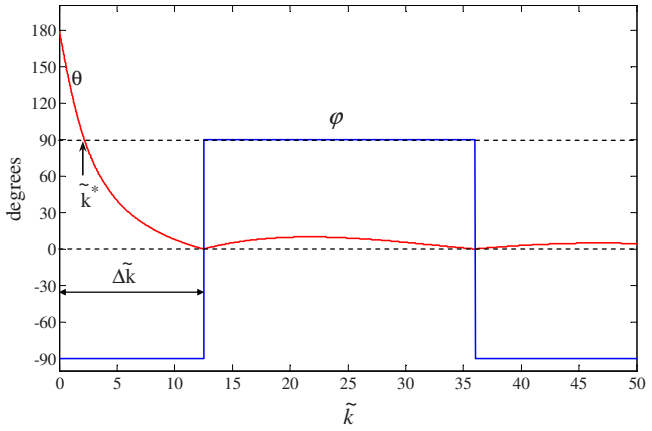

Fig. 4. Plot of the phase angles (φ,θ) for the spinor $|\psi(\mathrm{OUT})\rangle$ [Eq. (3)] associated to an electron incident on a resonant tunneling structure as a function of the reduced wave vector $\tilde{k}=k/k_0$. The parameters of the resonant tunneling structure are the same as in Fig. 3. $\Delta\tilde{k}$ is the minimum wave vector (in reduced units) needed to realize a spin flip from the south to north poles on the Bloch sphere. The zeros of θ are the locations of the quasibound state energies of the resonant tunneling structure.

$\Delta\tilde{k}$ indicated in Fig. 4 because it allows a full swing in θ from 0 to π, whereas the swing in θ is much smaller between the first two and higher resonances. The quantity $\Delta\tilde{k}$ is much smaller than the infinite change in $\tilde{k}$ needed for a single delta scatterer to realize an inverter, as discussed in Sec. IV B. Because $T=R$ for $\tilde{k}=\tilde{k}^*$, $\theta=\pi/2$, which is enough to implement the Hadamard gate using a resonant tunneling device.

These results can be extended to a superlattice, modeled as a sequence of evenly spaced identical delta function scatterers. In this case each resonant state present in the smaller unit with two scatterers leads to a passband for the infinitely periodic structure. In Fig. 5 we plot the transmission coefficient

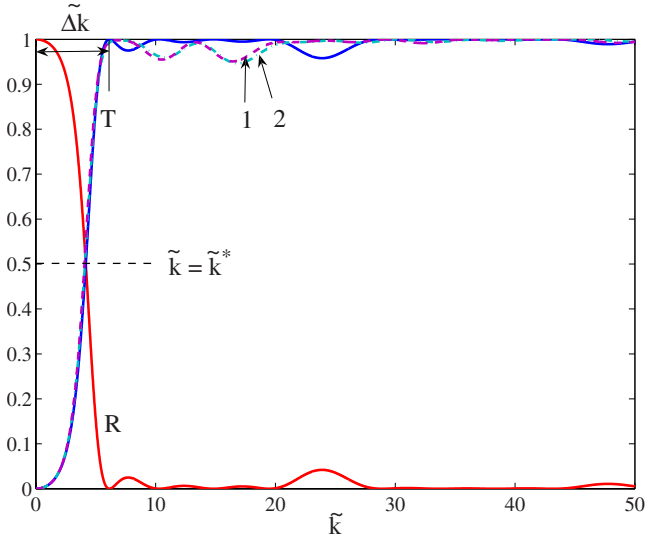

Fig. 5. Transmission T and reflection R coefficients versus $\tilde{k}=k/k_0$ for an electron incident from the left on a superlattice modeled as five delta function scatterers of strength V_I separated by a distance a ($V_I=0.3$ eV Å and $a=50$ Å). The curves labeled 1 and 2 are T versus $\tilde{k}$ for two imperfect superlattices, that is, for two arrays of five delta function scatterers whose positions are selected randomly over each interval of length 50 Å.

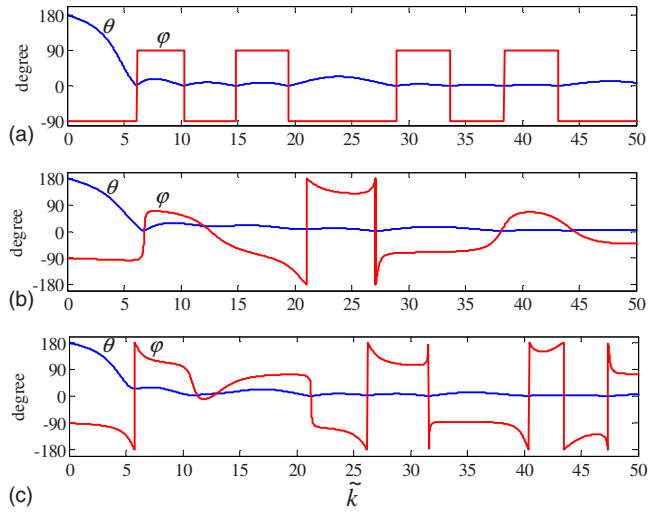

Fig. 6. (a) The reduced wave vector dependence of the phase angle (φ,θ) associated with the spinor $|\psi(\mathrm{OUT})\rangle$ describing tunneling across an array of five delta scatterers separated by 50 Å and with $V_I=0.3$ eV Å. The zeros in θ are where the transmission through the superlattice reaches unity. (b) and (c) The angles (φ,θ) for two random arrays of five elastic scatterers. The curves are very sensitive to the impurity configuration.

for a structure consisting of five delta function scatterers with the same parameters as for the resonant tunneling device we have described and with the same spacing of 50 Å between each scatterer. The transmission coefficient reaches unity at four values of $\tilde{k}$ in the interval,[5–25] which is a well known result for finite repeated structures.[24,25] Also the range $\Delta\tilde{k}$ needed to reach the condition $T=R$ is reduced compared to the case of a resonant tunneling device. As the number of periods in the superlattice increases, $\Delta\tilde{k}$ converges to a limit corresponding to the lower edge of the passband of the infinite superlattice. As shown in Fig. 6(a), the angle θ allows a full swing from the north the to south pole on the Bloch sphere over a range $\Delta\tilde{k}$, which is smaller than what is necessary for a resonant tunneling device, and the phase angle φ toggles back and forth between $-\pi/2$ and $\pi/2$ each time a resonance is crossed.

Figure 5 also shows a plot of the transmission coefficient (curves labeled 1 and 2) versus $\tilde{k}$ for two imperfect structures in which the locations of the five delta scatterers are chosen randomly over each interval of length a. The transmission coefficient is fairly sensitive to $\tilde{k}$ in the range of $\tilde{k}$ where the lower passband occurs for the infinite superlattice. However, the transmission curve is insensitive to the imperfections in the superlattice in the same range of $\tilde{k}$. As shown in Figs. 6(b) and 6(c), the angle θ is also insensitive to imperfections in the superlattice but the phase φ is not. The latter result is the compounded effect of multiple reflections between impurities and the sensitivity of φ to the exact impurity location in each section of length a.

D. Scattering through a periodic array of delta scatterers

The scattering matrix elements for the 1D periodic system (or superlattice) can be calculated exactly.[26–28] The transmission amplitude is found to be

$$t_N=\frac{e^{i(N-1)ka}}{D_N}, \tag{41}$$

and the reflection amplitude is given by

$$r_N=-i\frac{k_0}{k}\frac{e^{i(N-1)ka}}{D_N}\frac{\sin(N\Gamma a)}{\sin(\Gamma a)}, \tag{42}$$

where

$$D_N=e^{iNka}\left\{\cos(N\Gamma a)+i\,\mathrm{Im}\left[e^{-ika}\left(1+i\frac{k_0}{k}\right)\right]\frac{\sin(N\Gamma a)}{\sin(\Gamma a)}\right\}, \tag{43}$$

a is the distance between adjacent scatterers, and Γ is the quasimomentum. Γ is the solution of the transcendental equation,

$$\cos(\Gamma a)=\cos(ka)+\frac{k_0}{k}\sin(ka). \tag{44}$$

By using Eqs. (8)–(10), it can be shown that $\langle S_x\rangle=0$,

$$\langle S_y\rangle=-\hbar\,\mathrm{Re}(r^*t)=-\frac{\hbar}{1+(k_0/k)^2[\sin^2(N\Gamma a)/\sin^2(\Gamma a)]}\frac{\sin(N\Gamma a)}{\sin(\Gamma a)}\frac{k_0}{k}, \tag{45}$$

and

$$\langle S_z\rangle=\frac{\hbar}{2}(2|t|^2-1)=\frac{\hbar}{2}\left[\frac{2}{1+(k_0/k)^2[\sin^2(N\Gamma a)/\sin^2(\Gamma a)]}-1\right]. \tag{46}$$

For $N=1$ we recover Eqs. (33) and (34). For N delta scatterers the incident energies which satisfy the condition,

$$\frac{\sin(N\Gamma a)}{\sin(\Gamma a)}=0, \tag{47}$$

correspond to the transmission equal to unity, which occurs at values of the quasimomentum in the first Brillouin zone,

$$\Gamma_n a=\frac{\pi n}{N}, \tag{48}$$

with $(n=1,\ldots,N-1)$. At these values $\langle S\rangle=\langle S_y\rangle=0$ and $\langle S_z\rangle=\hbar/2$.

E. Transport through random arrays of delta scatterers

The analysis of Sec. IV E was extended to a large number of delta function scatterers of strength $V_I\delta(x-(x_0^i+(i-1)a))$, where V_I is chosen to be 0.3 eV Å and x_0^i is the location of the ith impurity located in the interval $[(i-1)a,ia]$. Each impurity location is generated using a uniform random number in each interval. The length of each subsection is set equal to 237 Å and the wave vector of the incident electron k is chosen such that $ka=\pi$ for an incident energy E of 10 meV and $m^*=0.067m_0$, the electron effective mass in GaAs.

Figure 7 is a plot of the phase angle θ of the spinor $|\psi(\mathrm{OUT})\rangle$ versus the number N of subsections crossed. The two top curves are θ versus N for two impurity configura-

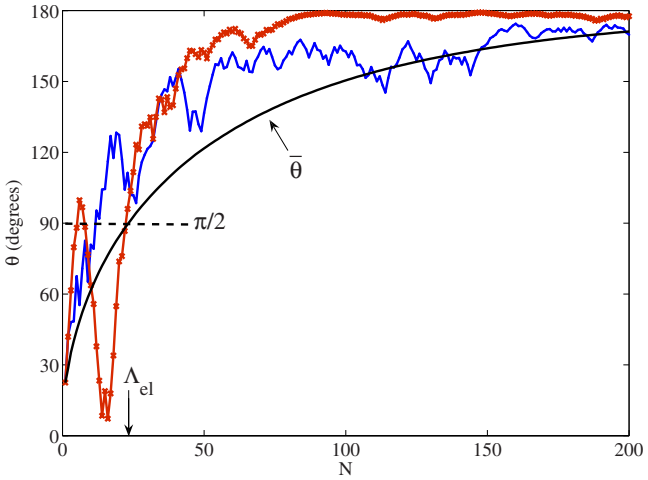

Fig. 7. Evolution of the angle θ for the spinor $|\psi(\mathrm{OUT})\rangle$ on the Bloch sphere as a function of sample length for two arrays of elastic scatterers (two top curves). The smoother curve represents the average of θ over an average of 10^5 arrays with the locations of each individual scatterer varied uniformly across each subsection of the array. The elastic mean free path Λ_{el} (in units of subsections crossed) is where $\bar{\theta}=\pi/2$. Here, $\Lambda_{\mathrm{el}}=23$.

tions. The curves show regions where θ decreases as N increases, which corresponds to an increase in the conductance of the array. This decrease in θ as N increases is pronounced for one of the two impurity configurations for $N<20$. A plot of the average value of θ over an ensemble of 10^5 samples is shown as the curve labeled $\bar{\theta}$ in Fig. 7. The quantity $\bar{\theta}=\pi/2$ for $N\approx 23$. For samples with this number of impurities, their average resistance is equal to h/e^2 and the elastic mean free path is equal to 23×237 Å≈ 0.55 μm.

The resistance of the random arrays versus the number of impurities crossed is plotted in Fig. 8. The latter was generated by first calculating the conductance of the sample using the Landauer formula,[23]

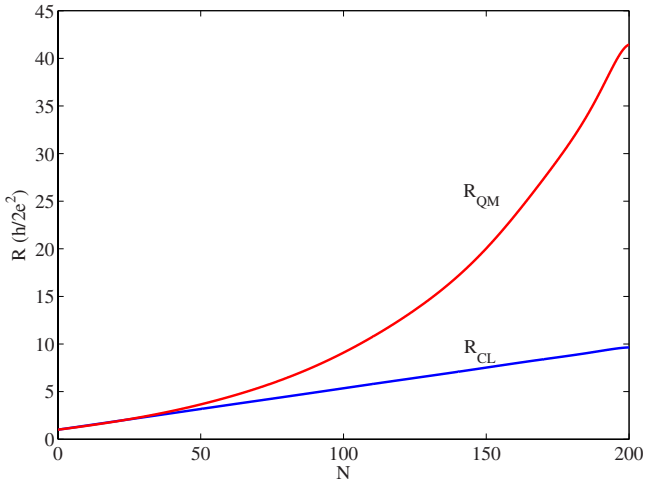

Fig. 8. Plot of the quantum-mechanical resistance R_{QM} calculated as $\langle G\rangle^{-1}$, where $\langle G_L\rangle$ is the average over an ensemble of 10^5 impurity configurations of the Landauer conductance as a function of the number of impurities crossed in the sample. Also shown is the value of the classical resistance R_{CL} neglecting the effects of multiple reflections between scatterers. The elastic mean free path Λ_{el} (in units of subsections crossed) is where R_{CL} reaches a value of $h/e^2\sim 23$ kΩ.

$$G_L=\frac{2e^2}{h}T, \tag{49}$$

where T is the transmission coefficient across the array calculated at the electron incident energy.

In Fig. 8 we show the results for the resistance $R=\langle G_L\rangle^{-1}$, where $\langle G_L\rangle$ is the average over a large number of samples. $\langle G_L\rangle$ was calculated using the rule for cascading scattering matrices associated with adjacent sections in a sample. The rule for cascading either the amplitude or the probability scattering matrices is outlined in Refs. 18 and 19. The latter neglects the effects of multiple reflections between the impurities and leads to Ohm's law, that is, the classical result R_{CL} which is expected to grow linearly with the number of impurities crossed. The quantum-mechanical result, R_{QM}, includes the effects of quantum interference and multiple reflections between impurities and leads to an exponential growth of R_{QM} versus length. The difference between the two curves in Fig. 8 occurs for a value of the resistance equal to h/e^2 (roughly 23 kΩ), which occurs for $N\approx 23$, or the sample length equal to the elastic mean free path. This exponential increase in the resistance was first predicted by Anderson in his pioneering work on the phenomenon of localization in disordered samples.[29] He showed that in strictly one-dimensional systems any plane wave incident from the contact decays exponentially in the sample no matter its incident energy and no matter how small the amount of disorder. This exponential decay of the wave function in the sample is the main reason for the exponential increase of R_{QM} with length.

V. CONCLUSIONS

The effective spin concept has also been used to describe the spatial correlations between reflection and transmission amplitudes of polarized photon beams from a combination of beam splitters, mirrors, and interferometers.[30–32] More recently, the effective spin concept has been used to examine the critical problem of entanglement between channels associated with propagating modes in mesoscopic systems, as reported in recent experiments by Neder *et al.*[17] and their theoretical interpretation by Samuelson *et al.*[33]

We have discussed an alternative description of phase coherent charge transport through mesoscopic systems in terms familiar to researchers in spintronics and quantum computing. The effective spin formalism provides a quantum computing approach to simple scattering problems and to localization in random arrays of elastic scatterers.

[1] Y. Imry, *Introduction to Mesoscopic Physics* (Oxford U. P., New York, 2002).
[2] S. Datta, *Electronic Transport in Mesoscopic Systems* (Oxford U. P., New York, 1995).
[3] M. Cahay and S. Bandyopadhyay, in *Advances in Electronics and Electron Physics*, edited by P. W. Hawkes (Academic Press, San Diego, 1994), Vol. 89, pp. 94–253.
[4] C. W. J. Beenakker and H. van Houten, in *Solid State Physics*, edited by H. Ehrenreich and D. Turnbull (Academic Press, Boston, 1991), Vol. 44, pp. 1–228.
[5] N. S. Yanofsky and M. A. Mannucci, *Quantum Computing for Computer Scientists* (Cambridge U. P., New York, 2008).
[6] P. Kaye, R. Laflamme, and M. Mosca, *An Introduction to Quantum Computing* (Oxford U. P., New York, 2007).
[7] M. A. Nielsen and I. L. Chuang, *Quantum Computation and Quantum Information* (Cambridge U. P., New York, 2000).

[8] S. Bandyopadhyay and V. P. Roychowdhury, "Switching in a reversible spin logic gate," Superlattices Microstruct. **22**, 411–416 (1997).
[9] L. A. Openov and A. M. Bychkov, "Non-dissipative logic device not based on two coupled quantum dots," Phys. Low-Dimens. Struct. **9–10**, 153–160 (1998).
[10] D. Loss and D. P. DiVincenzo, "Quantum computation with quantum dots," Phys. Rev. A **57**, 120–126 (1998).
[11] V. Privman, I. D. Wagner, and G. Kventsel, "Quantum computation in quantum-Hall systems," Phys. Lett. A **239**, 141–146 (1998).
[12] B. E. Kane, "A silicon-based nuclear spin quantum computer," Nature (London) **393**, 133–137 (1998).
[13] S. Bandyopadhyay, "Self-assembled nanoelectronic quantum computer based on the Rashba effect in quantum dots," Phys. Rev. B **61**, 13813–13820 (2000).
[14] T. Calarco, A. Datta, P. Fedichev, and P. Zoller, "Spin-based all-optical quantum computation with quantum dots: Understanding and suppressing decoherence," Phys. Rev. A **68**, 012310 (2003).
[15] A. E. Popescu and R. Ionicioiu, "All-electrical quantum computation with mobile spin qubits," Phys. Rev. B **69**, 245422 (2004).
[16] R. Ionicioiu, "Spintronics devices as quantum networks," Laser Phys. **16**, 1444–1450 (2006).
[17] I. Neder, N. Ofek, Y. Chung, M. Heiblum, D. Mahalu, and V. Umansky, "Interference between two indistinguishable electrons from independent sources," Nature (London) **448**, 333–337 (2007), and references therein.
[18] S. Datta, M. Cahay, and M. McLennan, "Scatter-matrix approach to quantum transport," Phys. Rev. B **36**, 5655–5658 (1987).
[19] M. Cahay, M. McLennan, and S. Datta, "Conductance of an array of elastic scatterers: A scattering-matrix approach," Phys. Rev. B **37**, 10125–10136 (1988).
[20] S. Bandyopadhyay and M. Cahay, *Introduction to Spintronics* (CRC Press, Boca Raton, FL, 2008).
[21] Using the unitary property of the scattering matrix, it can be easily checked that the trace of the matrix ρ is unity and ρ satisfies the following properties, $\rho^{\dagger}=\rho$, $\rho^2=\rho$, and $\mathrm{Tr}[\rho^2]=\mathrm{Tr}[\rho]=1$, which are all characteristics of the density matrix associated with a pure state (Ref. 7).
[22] Y. M. Blanter and M. Büttiker, "Shot noise in mesoscopic conductors," Phys. Rep. **336**, 1–166 (2000).
[23] R. Landauer, "Spatial variation of currents and fields due to localized scatterers in metallic conduction," IBM J. Res. Dev. **1**, 223–231 (1957).
[24] D. J. Vezzetti and M. Cahay, "Transmission resonances in finite, repeated structures," J. Phys. D **19**, L53–L55 (1986).
[25] M. Cahay and S. Bandyopadhyay, "Properties of the Landauer resistance of finite repeated structures," Phys. Rev. B **42**, 5100–5108 (1990).
[26] V. M. Gasparian, B. L. Altshuler, A. G. Aronov, and Z. H. Kasamanian, "Resistance of one-dimensional chains in Kronig-Penny-like models," Phys. Lett. A **132**, 201–205 (1988).
[27] V. Gasparian, "Transmission coefficient of an electron traveling across a one-dimensional random potential," Sov. Phys. Solid State **31** (2), 266–268 (1989).
[28] V. Gasparian, U. Gummich, E. Jódar, J. Ruiz, and M. Ortuño, "Tunneling and dwell time for one-dimensional generalized Kronig-Penney model," Physica B **233**, 72–77 (1997).
[29] P. W. Anderson, "Absence of diffusion in certain random lattices," Phys. Rev. **109**, 1492–1505 (1958).
[30] C. H. Holbrow, E. J. Galvez, and M. E. Parks, "Photon quantum mechanics and beam splitters," Am. J. Phys. **70**, 260–265 (2002).
[31] T. B. Pittman, B. C. Jacobs, and J. D. Franson, "Probabilistic quantum logic operations using polarizing beam splitters," Phys. Rev. A **64**, 062311 (2001).
[32] P. T. Cochrane and G. J. Milburn, "Teleportation with the entangled states of a beam splitter," Phys. Rev. A **64**, 062312 (2001).
[33] P. Samuelsson, I. Neder, and M. Büttiker, "Reduced and projected two-particle entanglement at finite temperatures," Phys. Rev. Lett. **102**, 106804 (2009).

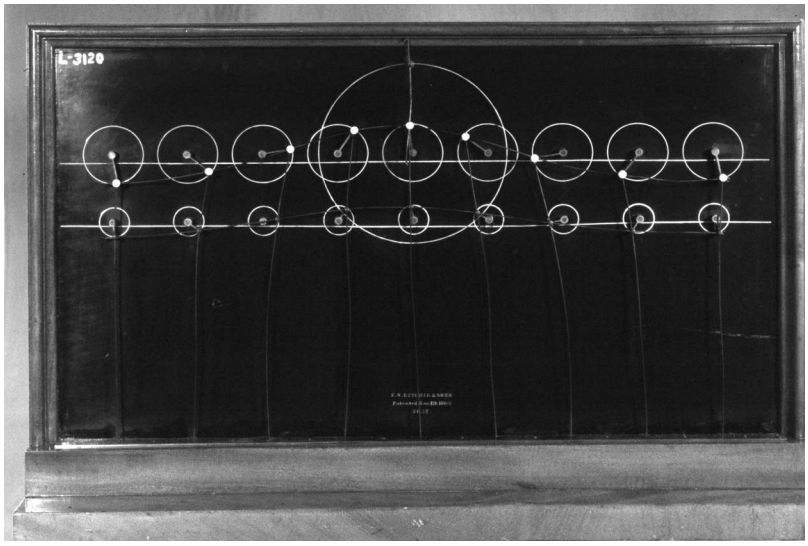

Lymans Water Wave Demonstrator. In 1868, Prof. Chester Smith Lyman, Professor of Industrial Mechanics and Physics in the Yale Scientific School, published a description of this wave machine. The patent was assigned to the Boston maker of physical instruments, E. S. Ritchie. Lymans wave machine demonstrated the motion of water molecules during the passage of deep-water waves. Viewed from above, the motion of a chip of wood floating on the surface of the water appears to be back-and-forth; to an observer at the side it moves up-and-down. These two motions compound to give a circular motion to the chip. The apparatus is at Yale University, and is listed in the 1869 Ritchie catalogue at $35.00. (Notes and photograph by Thomas B. Greenslade, Jr., Kenyon College.)